Interannual and seasonal variations in aerosol optical depth of the atmosphere in two regions of Spitsbergen Archipelago (2002-2018)

Dmitry M. Kabanov[1], Christoph Ritter[2], Sergey M. Sakerin[1]

[1]V.E. Zuev Institute of Atmospheric Optics, Siberian Branch, Russian Academy of Sciences, Academician Zuev Square 1, Tomsk, Russia
[2]Alfred Wegener Institute for Polar and Marine Research, 14473 Potsdam, Germany

Correspondence to: Christoph Ritter (christoph.ritter@awi.de)

Abstract. In this work hourly averaged sun photometer data from the sites Barentsburg and Ny-Ålesund, both located in Spitsbergen in the European Arctic, are compared. Our data set comprises the years 2011 to 2017. We found for more turbid periods (aerosol optical depth $\tau_{0.5} > 0.1$) that typically Barentsburg is more polluted than Ny-Ålesund, especially in the short wave spectrum. However, the diurnal variation of AOD is highly correlated. Next, τ was divided into a fine and coarse mode. It was found that generally the fine mode aerosol optical depth dominates and also shows a larger interannual as inner annual variation. The fine mode optical depth is in fact larger in spring during the Arctic Haze period. Overall the aerosol optical depth seems to decrease, although this is not statistically significant.

1 Introduction

The studies of the character and causes of variations in all components of climate system, including the aerosol composition of the atmosphere, became more urgent with regard to climate change [IPCC, 2013]. Atmospheric aerosol plays an important role in the processes of solar radiative transfer and exchange by different substances (and, in particular, pollutants) between the continents and ocean [e.g. Kondratyev et al., 2006]. As compared to gases, aerosol is characterized by a complex physicochemical composition and stronger variation of concentration and radiative impact.

Of the various aerosol characteristics, the observations of aerosol optical depth (AOD) of the atmosphere are most widespread and carried out at the international and national networks of stations using sun photometers (see, e.g., [WMO, 2005; Holben et al., 1998]). The AOD represents the extinction of radiation, integrated over atmospheric column, and can be considered as an optical equivalent of the total aerosol content.

One of the main aerosol climatology problems is to determine the specific features of interannual and seasonal variations in different regions. However, under the conditions of changing climate system, a time series 10 years (or even 20 years) long may turn out to be insufficient to identify correctly the tendencies or periodicities in variations of aerosol characteristics.

First observations of spectral AOD in the Arctic zone were carried out about 40 years ago [Shaw, 1982; Freund, 1983; Radionov and Marshunova, 1992]; however, they become regular in character only in the early 2000s, after the development

of photometric observations at continental stations. A comprehensive overview of atmospheric AOD in the Polar Regions has been presented by C. Tomasi [Tomasi et al., 2012; 2015].

Studies by various authors showed that the Arctic atmosphere is affected appreciably by outflows of aerosols of different types (smoke, industrial, sulfate, organic) from Eurasia and North America. The most powerful effect is due to smoke from forest

35 fires that cover large areas of boreal zone [e.g. Chubarova et al., 2012; Sitnov et al., 2013; Zhuravleva et al., 2017]. Long-range transports of smoke plumes lead to a considerable pollution of the Arctic atmosphere [Stohl et al., 2006; Stone et al., 2008; Eck et al., 2009; Vinogradova et al., 2015]. These episodes are short-term (1-3 days) and rare because they depend on the product of probabilities of two independent events: (a) the fire itself in any area of boreal zone, and (b) the fact that the trajectory of air transport from a fire center arrived exactly at a given region of the Arctic.

40 In addition to smokes, anthropogenic and other types of fine aerosol also outflow from midlatitudes. In contrast to forest fires, the sources of these aerosols operate almost all the time and are distributed over the entire territory of human life activity. A somewhat larger concentration of anthropogenic aerosol in densely populated regions of Europe was observed in the past century; however, recently the industrial emissions have been stabilized or reduced in this area [Tørseth et al., 2012; Li et al., 2014; Zhdanova et al., 2019].

45 An AOD increase may also be associated with volcanic activity. In the period of time considered here, there were no large eruptions (like Pinatubo volcano in 1991), having a global effect. The effects of less powerful volcanic eruptions on the Arctic atmosphere are short-term to mid-term (some weeks in duration) and comparable to those due to smokes from forest fires. For instance, AOD increase on Spitsbergen was observed after the eruptions of volcanoes Kasatochi (August 2008) and Sarychev (July 2009) [Hoffmann et al., 2010; Toledano et al., 2012].

50 The effects of pollutant outflows on the Arctic atmosphere intensify in late winter – early spring. The temperature inversions in this season lead to the formation and accumulation of aerosol in separate layers of the troposphere (the Arctic Haze Phenomenon) [e.g. Shaw, 1995; Quinn et al., 2007; Tomasi et al., 2015].

In the recent decade increasingly more work was published analyzing the multiyear AOD variations in different regions, either based on spectral [Zhdanova et al., 2019; Chubarova et al., 2016; Putaud et al., 2014; Li et al., 2014; Xia, 2011; Michalsky et

55 al., 2010; Sakerin et al., 2008a; Weller et al., 1998] or integrated (actinometric) [Gorbarenko and Rublev, 2016; Plakhina et al., 2009; Ohvril et al., 2009] measurements of solar radiation. In most regions of Eurasia the AOD shows a decreasing tendency following 1995. The negative AOD trend is associated with decreasing anthropogenic load and the absence of powerful volcanic eruptions analogous to Pinatubo (July 1991) and El Chichón (March – April 1982). Of particular interest is the dynamics of aerosol constituent of the atmosphere in the Arctic zone where there are the largest climate changes [IPCC,

60 2013]: increased temperature and prolonged warm period, reduction of sea-ice area, changes in the circulations, etc.

The archipelago of Spitsbergen in the European Arctic is a special region because it is strongly influenced by the warm West Spitsbergen Current. Hence, for the given geographical latitude the West Coast of Spitsbergen faces warm and moist conditions. (Walczowski and Piechura, 2017). Moreover, Spitsbergen currently faces a pronounced winter warming of about 2 degrees per decade, which can partly be explained by more efficient advection from the Atlantic Ocean (Isaksen et al., 2015;

65 Dahlke and Maturilli, 2017). For this reason aerosol properties over Spitsbergen may not be directly comparable to aerosol observations at other Polar sites. On the other hand, we may see aerosol properties at Spitsbergen now which are more typical for the Arctic in the future in warmer, more marine conditions.

For Spitsbergen an analysis of aerosol properties for separate periods was already performed before [Herber et al., 2002; Glantz et al., 2014; Chen et al., 2016; Pakszys and Zielinski, 2017]. In this work, we discuss the AOD measurements in 2002-2018 in

70 two regions of Spitsbergen: Ny-Ålesund and Barentsburg. Based on the multiyear observation time series, we considered the following issues: (a) differences in AOD between neighboring regions; (b) choice of the method for extracting the contributions of two (fine and coarse) AOD components; (c) seasonally average AOD variations during the polar day; and (d) the specific features of the interannual AOD variations during two periods of measurements (2002-2010 and 2011-2018).

2 Instruments, methods, and observational data

75 ### 2.1 Characterization of instruments and regions of measurements

Historically, observations of the spectral AOD $\tau^a(\lambda)$ on Spitsbergen Archipelago are carried out at three closely lying scientific stations (in the order of decreasing latitude): Ny-Ålesund (78°54′N, 11°53′E), Barentsburg (78°04′N, 14°13′E), and Hornsund (77°00′N, 15°34′E). The distances from Barentsburg to Ny-Ålesund and Hornsund are 110 and 120 km respectively.

Measurements of atmospheric AOD in the scientific settlement Ny-Ålesund (population of about 100 residents during summer)

80 have been performed since 1991. At the first stage (1991-1999) the observations were performed in separate periods of the year (polar day, polar night) using photometers of different types (Sun, Moon, Star). The results of those studies were considered in [Herber et al., 2002]. Here, we analyze the AOD variations in a later period when measurements became regular and homogeneous in character. The main characteristics of sun photometers (SP1A and SP2H), used in measurements, are presented in Table 1.

85 The sun photometer in Ny-Ålesund is located just south of the settlement in about 10m asl on the BSRN radiation field. The temporal resolution of the data is 1 minute. The instruments are regularly calibrated in Izaña /Tenerife. The air masses for aerosol and for ozone were considered according to the formulas by Kasten and Young (1989) and the WMO No 183 report (2008), respectively. A cloud screening similar to Alexandrov et al. (2004) has been performed.

90

Table 1. Characteristics of Sun-photometers and data volume in Ny-Ålesund and Barentsburg

Scientific stations	Sun-photometers	Angle of view, degrees	Range of spectrum // number of spectral channels	Number of hours (days) of measurements
Ny-Ålesund (AWI, Germany)	SP1A, SP2H	1	0.37-1.06 μm // 13 0.37-1.05 μm // 12	7520 (1130)
Barentsburg (AARI and IOA SB RAS, Russia)	SPM, SP-9	< 2,5 < 2	0.34-2.14 μm // 11 0.34-2.14 μm // 13	1732 (350)

95

In 2011 the monitoring of aerosol characteristics (including AOD [Sakein et al., 2018a]) was organized in the Russian Scientific Center, located in the southwestern part of Barentsburg settlement on the coast of Grønfjorden Gulf. Products of coal-mining industry and thermal power plant, located at distance of about 1 km, may influence the aerosol characteristics in Barentsburg (population of about 500 residents).

100 The atmospheric AOD was initially measured using SPM portable sun photometer [Sakein et al., 2013] at an altitude of 65 m above sea level. In 2015 it was changed to SP-9 photometer with automatic Sun tracking system (the instrument was installed at the altitude of 74 m). The base set of the wavelength channels comprises the interference filters with the passband maxima at the wavelengths: 0.34, 0.37, 0.41, 0.50, 0.55, 0.67, 0.77, 0.87, 1.04, 1.25, 1.55, and 2.14 μm. Still another wavelength channel (0.94 μm) is used to determine the total water vapor content of the atmosphere.

105 The method for calculating the spectral AOD [Kabanov and Sakerin, 1997; Kabanov et al., 2009] includes accounting for the spectral transmission functions of light filters, and Rayleigh scattering and absorption by atmospheric gases: H_2O, O_3, CO_2 and others. The absorption is calculated using the databases of spectral line parameters HITRAN-2000 (http://www.hitran.com), models of continual absorption MT_CKD (http://rtweb.aer.com/continuum_code.html) and vertical gas distribution AFGL [Anderson et al., 1986]. Water vapor absorption is accounted for using real water vapor contents, 110 measured in the wavelength channel of 0.94 μm.

Total amount of data (hours and days of measurements), which were used in the AOD analysis in two regions, is presented in Table 1. Seasonal and interannual AOD variations were analyzed for the period of polar day (March-September). First the hourly average AOD values were used to calculate the averages for each day of measurements, then the monthly averages were calculated, based on which the averages for each year (or, more specifically, from March to September) were determined. 115 For brevity, they will be called Daily, Monthly, and Annual AOD. The interannual variations in AOD were estimated in two variants: (a) according to the average values in the measurement period (Annual AOD); and (b) according to the averages in periods of spring maximum and autumn minimum of AOD.

2.2 Data comparison and preparation of observation time series

A comparison of observations using two photometers may be of interest for intercalibration of the instruments, i.e., estimating instrumental-methodic AOD determination errors (for the Polar Regions e.g. Mazzola et al. 2011). If the measurements are separated in space (as in the given case), the difference in the data makes it possible to estimate the local AOD inhomogeneities (Sakerin et al. 2010), caused by anthropogenic or natural factors: local weather conditions, type and state of the underlying surface, orography, and the effect of industrial or other sources of aerosol.

It should be noted that we already compared earlier the AOD measurements at the neighbouring stations on Spitsbergen Archipelago, i.e., Hornsund and Ny-Ålesund [Toledano et al., 2012; Pakszys and Zielinski, 2017]. Comparison of time independent measurements showed that the average difference in the annual and seasonal AOD values at the wavelength of 0.55 μm does not exceed 0.01-0.02. Large differences in AOD between these stations occur in periods of Arctic haze and outflows of smokes from forest fires, which are differently manifested in these two regions. However, a comparison of monthly averages may introduce a bias due to different data availability at the involved sites.

In contrast to the above-mentioned works, we compared quasi-synchronous (nearly time coincident) AOD measurements in the neighbouring regions in 2011-2017 (see [Kabanov et al., 2018] for more details). The data of the SP1A (Ny-Ålesund) and SPM (Barentsburg) photometer observations were used to calculate the hourly average AOD values. Then, the datasets from the two regions were "juxtaposed" provided that the times of the AOD measurements differed by no more than one hour.

Comparison of measurements with the two photometers showed a large dispersion of the data under the conditions of strong atmospheric turbidities, namely, during outflow of smoke plumes from forest fires and in the Arctic Haze situations. Due to large spatial inhomogeneity of these structures, AOD, measured in two regions, may strongly differ, making the comparison incorrect. Therefore, further analysis was performed for usual situations, when τ^a (0.5 μm) < 0.2. Figure 1 illustrates the regression relation between τ^a (0.5 μm) measurements in the neighbouring regions of Spitsbergen.

A comparison of the statistical characteristics showed that the average AOD values are a little larger in Barentsburg than in Ny-Ålesund [Kabanov et al., 2018]. The maximum difference in AOD is observed in the shortwave part of the spectrum (0.38 μm), $\Delta = \tau^a$ (SPM) – τ^a (SP1A) = 0.024; while in IR range (0.87μm) the difference decreases to Δ = 0.005. This feature is real despite the decreasing AOD at longer wavelengths and indicates that fine aerosol is more abundant in the atmosphere of Barentsburg. At the same time, we note that the AOD differences are minor (comparable with uncertainty of determining AOD – about 0.01-0.02 [Kabanov et al. 2009; Sakerin et al., 2013]), and the interdiurnal AOD variations in the two regions are coordinated in character (correlation coefficients are 0.83-0.89). Comparison of quasi-synchronous AOD measurements in Barentsburg and Hornsund gave close results [Kabanov et al., 2018]: $\Delta = 0.004 – 0.024$, the correlation coefficients are 0.71-

150   0.81. Hence, observations in the neighbouring regions on Spitsbergen are quite compatible and identically reflect the specific features of the AOD variations.

The joint use of results from AOD monitoring in the neighbouring regions makes it possible to control the reliability of information, as well as to identify the specific features of AOD variations not only for a specific site, but for the region as a whole. The results of the observations in each of the regions have their own advantages. The advantage of the data from

155   Barentsburg (SPM / SP-9 photometers) is a wider range (0.34-2.14 μm) of the spectral measurements and the possibility to separate the contributions from two AOD components, using an empirical method (see subsection 2.3).

The valuable feature of the data from Ny-Ålesund is a longer AOD observation time series. However, different errors have been accumulated in these data for the long period of measurements. A simple exclusion of all suspect AOD measurements was undesirable because for analysis of multiyear variations it was necessary to keep the observation time series as long as

160   possible. Taking this circumstance into account, the multiyear observation time series was prepared for sorting out or correction of suspect AOD values [Kabanov et al., 2019a]. The initial dataset was processed to remove the data in which short-term bursts or rapid AOD variations were observed, as well as the distortions to smoothness of the wavelength dependences $\tau^a(\lambda)$. Owing to a certain redundancy of the number of spectral channels, we could identify false measurements and select most reliable data.

2.3 Fine and coarse AOD components

165   The attenuation of radiation by atmospheric aerosol varies as a function of wavelength, depending on sizes and refractive index of aerosol particles. To characterize the AOD, measured at different wavelengths, the Ångström formula is widely used:

$$\tau^a(\lambda) = \beta \cdot \lambda^{-\alpha},$$
(1)

where β and α are the approximation parameters of the spectral dependence of AOD; β is the turbidity coefficient, which is close in value to AOD at the wavelength of 1 μm; and α is the selectivity exponent (power-law decay).

170   Numerous studies in different regions and atmospheric conditions showed that the formula (1) does describe well the wavelength dependence $\tau^a(\lambda)$ in the main range (0.34 – 1 μm) of AOD measurements. [Angstrom, 1964; Shifrin, 1995; Eck et al., 1999; Cachorro et al., 2000; Schuster et al., 2006]. At the same time, the use of this formula has limitations and disadvantages, requiring an explanation.

First, the Ångström formula becomes unsuitable for describing the wavelength behavior of AOD in the atmospheric

175   "transparency windows" in the wavelength range of 1 – 4 μm. This is because the power-law dependence (1) stems from the combined action of fine and coarse aerosol fractions, which have different spectral properties. Extinction of radiation by small particles ($2\pi r/\lambda < 1$) is dominant in the visible region of spectrum; however, it rapidly decays with the growing wavelength and becomes insignificant in the region beyond of 1 μm. Extinction of radiation by coarse aerosol barely changes with the wavelength and becomes predominant in the IR range. Mie calculations and experimental data [Sakerin and Kabanov, 2007a;

180   Sakerin et al., 2008b] confirm that the power-law AOD decay gradually goes over into almost neutral dependence. Therefore, $\tau^a(\lambda)$ in a wider wavelength range is better to represent by a sum of two components:

$$\tau^a(\lambda) = \tau^c + \tau^f(\lambda) = \tau^c + m \cdot \lambda^{-n},$$

(2)

where τ^c is the constant (wavelength independent) coarse AOD component; $\tau^f(\lambda)$ is the selective fine component; m and n are the approximation parameters of the spectral dependence of $\tau^f(\lambda)$ (they are similar to the parameters β and α of the Ångström formula)

Second, the Ångström parameters do not allow one to interpret the causes for AOD variations unambiguously. An increase/decrease in the exponent α is sometimes unjustifiably attributed only to changes in fine aerosol. In fact, the exponent α conceals the actions of a few factors. The wavelength dependence of AOD is indeed determined by the optical properties of fine component $\tau^f(\lambda)$. Both the sizes and refractive index of small particles influence the degree of wavelength decay of AOD (and values of the parameters n and α). But, precisely what caused changes in the selectivity of AOD is almost impossible to determine without the use of additional information like e.g. aerosol in-situ measurements.

The next uncertainty factor is that the exponent α depends on the *relationship* of the optical depths of fine and coarse aerosol (τ_λ^f / τ^c). That is, α may increase both due to growing content of fine aerosol, and to decreasing content of coarse aerosol.

The presence of the interrelation between α and (τ_λ^f / τ^c) is illustrated in Fig. 2. The correlation coefficient between α and ln [(τ_λ^f / τ^c)+ 1] is statistically significant and equal to 0.68 (confidence level P < 0.0001).

We also note that the component τ^c, which influences the exponent α, is tightly related and has close values to the second Ångström parameter [Sakerin and Kabanov, 2007a, b]: $\tau^c \approx \beta$. A consequence of this is that the parameters α and β are themselves correlated.

Thus, the use of the Ångström parameters in the analysis of AOD variations is ambiguous and may lead to erroneous conclusions. It is more preferable to consider the specific features of variations in two AOD components: $\tau^f(\lambda)$ and τ^c. In addition to different sizes and spectral properties, fine and coarse aerosol fractions differ in the origins of particles and their transformation in the atmosphere. Fine (sulfate, organic, etc.) aerosol is formed in the atmosphere as a result of various photochemical and microphysical processes [Kondratyev et al., 2006]. The lifetime of fine aerosol in the troposphere is a few days; therefore, it can be transported long distances (hundreds and thousands of kilometers) away. The main source of coarse (marine and dust) aerosol is the underlying surface. Because of its short lifetime and small transport distance, coarse aerosol is more local in character and pertains to a specific terrain. The only exceptions are powerful dust outflows in tropical latitudes.

2.4 Methods for determining fine and coarse AOD components

As was already indicated above, in the IR range, the effect of fine aerosol becomes insignificant, and AOD is determined only by the coarse component. Therefore, τ^c can be determined by an empirical method (EM), i.e., from minimal or average AOD

values, measured in the range of 1.24-2.14 μm [Sakerin and Kabanov, 2007b; Sakerin et al., 2008b]. Then, the second (fine) component is found as a residual of the total AOD. Usually, it is estimated for the wavelength of 0.5 μm: $\tau_{0.5}^f = \tau_{0.5}^a - \tau^c$.

However, most sun photometers (and in particular the SP1A in Ny-Ålesund) operate in the wavelength range up to 1.05 μm, making *empirical* method inapplicable. In this case, τ^c and $\tau_{0.5}^f$ can be estimated using calculation methods. For instance, in the AERONET system (http://aeronet.gsfc.nasa.gov), $\tau_{0.5}^f$ is calculated using the spectral deconvolution algorithm [O'Neill et al., 2003], based on the relationship of spectral AOD, measured in the shortwave part of the spectrum 0.38-1.02 μm.

In the work [Kabanov and Sakerin, 2016] we suggested simpler methods for separating the contributions from $\tau_{0.5}^f$ and τ^c, based on the regression interrelations with the parameters of Ångström formula. In the first regression method (RM1), τ^c is estimated using its interrelation with the parameter β (see formula (3) below). In the second method (RM2), the regression dependence of $\tau_{0.5}^f$ on the parameters α and β (see formula (4)) is used. Comparison of different methods of $\tau_{0.5}^f$ (or τ^c) estimation for the conditions of the marine and continental (Tomsk) atmosphere showed close results: the average difference of τ^c from data of base *empirical* method (EM) does not exceed 0.007 for the standard deviation from 0.006 to 0.024.

For the conditions of Arctic region (Spitsbergen), we performed an additional study [Kabanov et al., 2019a], concerning the selection of an optimal method of $\tau_{0.5}^f$ (or τ^c) estimation. Different methods were tested using SPM photometer measurements of AOD in Barentsburg. The error of the methods was estimated by comparing the calculated values of $\tau_{0.5}^f$ or τ^c with the data from base *empirical* method.

Figure 3 illustrates the results of testing two regression methods (RM1 and RM2), based on the interrelations (a) between τ^c and the parameter β, and (b) between $\tau_{0.5}^f$ and the parameters α, β. For the conditions of Spitsbergen, we obtained the following regression equations:

RM1: $\tau^c = 0.665 \cdot \beta - 0.0005$ (3)

RM2: $\tau_{0.5}^f = (-0.829 + 1.066 \cdot 0.5^{-\alpha}) \cdot \beta$ (4)

Table 2 presents the standard deviations σ and the correlation coefficients R between the calculated (RM1, RM2) and empirical (EM) τ^c values. These results suggest the regression methods make it possible to estimate τ^c with an identical error of 0.007.

The disadvantage of the regression methods is that they require a preliminary data accumulation under the conditions of a specific region for determining optimal regression coefficients in equations (3) and (4) [Kabanov and Sakerin, 2016]. Of course, the error of the regression methods may increase if aerosol characteristics strongly differ from those typical for the region and do not correspond to the selected regression coefficients.

Therefore, in addition to the regression methods, we considered the applicability of another two methods of $\tau_{0.5}^f$ estimation, based on the results of solving the inverse problem, namely: retrieval of particle sizes from measurements of spectral AOD.

The inversion method 1 (IM1) is based on the interrelation between $\tau_{0.5}^f$ and volume or cross section of particles of fine aerosol. This method is implemented in the following steps:

1st step: Based on any known method of solving the inverse problem (for a specified refractive index, type of the particle distribution function, and grid of radius ranges), the spectral AOD values are used to calculate the particle distribution function (dV/dr) or (dS/dr).

2nd step: In the distribution (dV/dr) thus obtained we select its part referring to the fine fraction, and, for it, calculate the total particle volume (V^f) through integration.

3rd step: We consider the regression interrelation between particle volumes in the fine fraction (V^f) and the τ^f values, calculated by empirical method (EM). The interrelation thus obtained (Fig. 4a) is used to select the parameters of a linear regression equation which makes it possible to calculate the component τ^f according to the particle volumes V^f.

The inversion method 2 (IM2) is implemented by solving first the inverse problem, and then the direct problem of the aerosol optics: (a) as in IM1, the spectral AOD values are used to retrieve the distribution functions (dS/dr); and (b) based on the (dS/dr) values, $\tau_{0.5}^f$ is calculated for the size range of fine aerosol.

The inverse problem on retrieving the distribution functions (dS/dr) was solved using iteration algorithm of M.A. Sviridenkov [Sviridenkov, 2001], modified from Twitty algorithm [Twitty, 1975]. The particle distribution was assumed to be lognormal, and the refractive index was assumed to have the real part of 1.5 and the imaginary part of 0. In the calculations we used the following radius grid: 0.09-0.13-0.17-0.21-0.25-0.29-0.33-0.37-0.41-0.45-0.49-0.53-0.59-0.65-0.81-0.99-1.21-1.59-1.81-2-2.5-3 μm.

Applicability of inversion methods was estimated for a few variants: (a) for different wavelength intervals of AOD (0.34-2.14 μm; 0.38-0.87 μm; 0.38-1.02 μm; and 0.34-1.02 μm); (b) for the distribution functions (dS/dr) and (dV/dr); and (c) for different radius boundaries of particles of fine fraction (0.1-0.5 μm and 0.1-0.45 μm). Figure 4 presents examples of interrelations: (a) between $\tau_{0.5}^f$ (EM) and calculated values of particle volume V^f; and (b) between $\tau_{0.5}^f$ values, determined using base (EM) and inversion (IM1) methods. The calculations in this case were performed for the wavelength range of AOD 0.38-1.02 μm and particle radius range of 0.1-0.5 μm.

Analysis of application of IM1 and IM2 [Kabanov et al., 2019a] showed that the $\tau_{0.5}^f$ determination error decreases by about a factor of 1.5 when the AOD is used in a wide (0.34-2.14 μm) wavelength range. However, for the narrower wavelength range of the SP1A photometer (0.38-1.02 μm) the $\tau_{0.5}^f$ calculation error is comparable with results from regression methods (see Table 2). That is, the relative errors of the τ^c and $\tau_{0.5}^f$ calculations for the mean conditions of Barentsburg ($\tau_{0.5}^a = 0.086$ [Sakerin et al., 2018a]) are 30% and 11% respectively.

The IM1 method was chosen for a subsequent use. Despite a more complicated procedure of its calculations, IM1 is more sensitive to aerosol variations, which is indicated by the highest correlation coefficient between $\tau_{0.5}^{f}$ (IM1) and data from base (EM).

There may be a question as to why after retrieval of aerosol size distribution we nonetheless consider the seasonal and interannual variations in optical characteristics: τ^{c} and $\tau_{0.5}^{f}$? Analysis of disperse composition of aerosol is a more complex and non-unique problem because it is necessary to consider the transformation of two aerosol fractions, which are described by a few parameters: shapes and widths of distributions for each fraction, separation boundary, and effective particle radii. Moreover, an uncertainty remains about the values of these parameters because of the priori specified aerosol refractive index. In this work, we pursued a simpler task: to determine the character and magnitude of variations in aerosol optical characteristics. In this case, instead of many microstructure parameters, it is sufficient to analyze their more compact optical image in the form of two components, τ^{f} and τ^{c}.

Table 2. Estimates of applicability of different methods (RM1, RM2, IM1, IM2) of the τ^{c} (or $\tau^{f}_{0.5}$) calculation

Parameter	RM1	RM2	IM1	IM2
σ	0.007	0.007	0.007	0.008
R	0.819	0.963	0.967	0.953

3. Discussion of the results

Current climate change and environmental transformation influence the regularities of variations in aerosol characteristics to some degree. Because of the deficit of its own aerosol sources in the Arctic zone, an important role in AOD variations is played by outflows of smoke, anthropogenic and volcanic aerosol from midlatitudes. The frequency of these outflows in particular months and years determines the specific features of seasonal dynamics of AOD in Arctic regions and magnitude of interannual oscillations.

3.1 Interannual variations

The highest atmospheric turbidities in the region of Spitsbergen were observed on July 10, 2015 and on May 2-3, 2006 (Fig. 5). Daily AOD (0.5 μm) in these cases reached 0.82 and 0.6, about an order of magnitude lager than multiyear averages. After passing to monthly AOD values, the effect of these short-term turbidities decreased to 0.192 in May 2006 and 0.152 in July 2015. Trajectory analyses of air mass motion showed that the extreme AOD values in July 2015 were due to long-range transport of smokes from forest fires in Alaska [Sakerin et al., 2018a, Pakszys and Zielinski, 2017; Markowicz et al., 2016]. We also considered in detail the second anomalous situation (in May 2006) [e.g. Myhre et al., 2007; Stohl et al., 2007], associated with the outflow of smoke aerosol from agricultural fires in the Eastern Europe.

Episodes with high atmospheric turbidities were also observed in June 2003, March and August 2008, in April and August 2009, and in April 2011. The AOD values in these periods of time had already been analyzed by many authors [Toledano et al., 2012; Glantz et al., 2014; Tomasi et al., 2015; Chen et al., 2016; Pakszys and Zielinski, 2017]. Independent of the causes for these short-term turbidities (Arctic haze, outflows of smoke or volcanic aerosol), they enhance not only the monthly, but also annual AOD values.

The above-mentioned high-turbidity episodes (2006, 2008, 2009, 2015) were reflected partly in annual AOD oscillations (Fig. 6). Moreover, a maximum appeared in the interannual variations in 2011-2012. This maximum was due not to extreme 1-3-day AOD bursts, but to stronger turbidities as compared to the neighbouring years.

The annual AOD maxima occur with the average periodicity of about three years. When high-turbidity episodes are eliminated (see dashed line in Fig. 6), certain maxima disappear; however, the general character of the AOD oscillations remains unchanged. Among these maxima, the highest AOD value in 2003 seems suspect. This annual AOD value cannot be considered as representative because of short period of observations (4 days in March and 5 days in May-June) in this year.

In addition to oscillations, a tendency for a minor AOD decrease can be discerned in the multiyear variations. This is also indicated by a comparison of AOD characteristics in two periods of observations: the average AOD (0.5 µm) in 2011-2018 decreased by 0.013 relative to 2002-2010 (Fig. 5). However, this decreasing AOD tendency is not statistically significant. The statistical estimates of $\tau_{0.5}^f$ and τ^c variations in spring and fall periods in these two regions (Fig. 7) also revealed no trend component.

From the statistical characteristics (Table 3) and Fig. 7 it follows that AOD and its interannual variations are determined mainly by fine aerosol: the SD values and the range <Min – Max> are a factor of 2-3 larger for $\tau_{0.5}^f$ than τ^c. The relative variations $\tau_{0.5}^f$ and τ^c are about the same: their variation coefficients V are 14-29%. Neither AOD component shows a clear predominance of variation coefficients. For instance, in the period of 2011-2018, the variation coefficients were larger for $\tau_{0.5}^f$ than τ^c (25 and 20%) in Ny-Ålesund and with a reverse relationship (14 and 23%) found in Barentsburg.

The interannual oscillations in the Ångström exponent can be considered as minor: the variation coefficients for α are 13-15%. The average α and the total variability range (from 1 to 1.7) are in the regions of values characteristic for the continental midlatitude atmosphere and are larger than in the marine atmosphere [Sakerin et al., 2008b; 2018b]. These values of the Ångström exponent are because the ratio ($\tau_{0.5}^f / \tau^c = 2.6$-2.9) and the relative contribution of fine component ($\tau_{0.5}^f / \tau_{0.5}^a = 0.73$-0.75) are close to continental values. As an example, we present multiyear data in boreal zone of Siberia in spring (smoke-free) period [Kabanov et al., 2019b]. The average AOD values in Siberia are about two times larger ($\tau_{0.5}^f = 0.105$, $\tau^c = 0.036$) than in Ny-Ålesund, and the ratio ($\tau_{0.5}^f / \tau^c$) and the exponent α are almost the same: ($\tau_{0.5}^f / \tau^c$) = 2.92 and $\alpha = 1.43$.

Table 3. Statistical characteristics of Annual AOD: average, minimal (Min), maximal (Max) values, standard deviations (SD), and variation coefficients (V); values for Ny-Ålesund (2002-2018) in the first row, for Ny-Ålesund (2011-2018) in the second row; and for Barentsburg (2011-2018) in the third row

Parameters	Mean	SD	Min	Max	V, %
$\tau_{0.5}^{a}$	0.067	0.017	0.04	0.10	25
	0.059	0.012	0.04	0.08	20
	0.080	0.007	0.07	0.09	10
$\tau_{0.5}^{f}$	0.050	0.013	0.02	0.07	26
	0.044	0.011	0.02	0.06	25
	0.058	0.008	0.04	0.07	14
τ^{c}	0.017	0.005	0.01	0.03	29
	0.015	0.003	0.01	0.02	20
	0.022	0.005	0.01	0.03	23
α	1.41	0.19	1.03	1.71	13
	1.44	0.21	1.11	1.71	15
	1.24	0.19	1.01	1.60	15
β	0.026	0.008	0.016	0.040	31
	0.022	0.006	0.016	0.034	27
	0.035	0.005	0.025	0.042	14

From Figs. 6 and 7 it is clearly seen that AOD in Barentsburg is almost always higher than in Ny-Ålesund. The average excess of annual AOD is (see rows 2 and 3 in Table 3): $\Delta\tau_{0.5}^{a} = 0.02$, $\Delta\tau_{0.5}^{f} = 0.012$, $\Delta\tau^{c} = 0.008$. This result indicates that a little more anthropogenic (fine) and coarse aerosols are contained in the atmosphere of Barentsburg (see also Figs. 1 and 5).

Variations in annual AOD in Ny-Ålesund and Barentsburg are coordinated in character. Oscillations in fine component sometimes show opposite changes in the two regions, such as in spring 2013 (see Fig. 7). Different behaviors of $\tau_{0.5}^{f}$ may be because observation time series are inhomogeneous in each region due to clouds or because AOD are measured at different times.

3.2 Specific features of seasonal variations

The most common regularity of the seasonal AOD behavior at midlatitudes is the spring (and sometimes also summer) maximum and fall minimum [e.g., Sakerin et al., 2015; Chubarova et al., 2014; Holben et al., 2001]. The primary causes for this AOD behavior are the annual cycle in the Sun's declination meaning a return of sunlight and possibly a longer aerosol life-time over the frozen ocean. The springtime increases in insolation and temperature trigger a few processes: (a) snow cover evaporates and melts; (b) the atmosphere is enriched by different deposition products, accumulated over the winter, (c) primary (marine, soil) aerosol starts to come from the underlying surface; and (d) photochemical processes of production of in situ aerosol in the atmosphere and emission of organic aerosol are activated [e.g., Kondratyev et al., 2006].

The seasonal AOD dynamics in the Arctic zone is analogous to midlatitudes: springtime maximum and a decay toward fall [e.g., Toledano et al., 2012; Tomasi et al., 2015; Sakerin et al., 2018]. This AOD behavior is because of similar annual rhythms of both own aerosol sources in the Arctic and long-range aerosol transports from midlatitudes.

Figure 8 shows the seasonal variations in monthly AOD for two regions in Spitsbergen. The seasonal AOD behaviours in Ny-Ålesund were similar in character in 2002-2010 and 2011-2018. The difference is that AOD values in March-June have decreased by ~0.02 in recent 8 years. At the same time, monthly AOD in the second half of polar day (July-September) remained at the same level of low values 0.05-0.06. As a result, the seasonal AOD decrease in 2011-2018 became less pronounced: the relative amplitude had been 30% (versus 55% in the period of 2002-2010).

Seasonal AOD variations in Barentsburg are characterized by an additional summer maximum in July-August. Despite this difference, common factors in AOD variations in the two regions are nonetheless predominant. Analysis of interrelation between AOD values, measured in Ny-Ålesund and Barentsburg (Fig. 9), showed quite a high (0.90) correlation coefficient. Hence, the synoptic, seasonal, and interannual AOD oscillations are largely coordinated in character.

Observation time series in the two regions were compared to clarify the causes for the summertime AOD maximum in Barentsburg. The increased AOD values in July and August were found to be due to the situations with smoke outflows (and, in particular, on July 10, 2015 [Sakerin et al., 2018a]). Of the total number of measurements, percentage of smoke-contaminated measurements turned out to be larger in Barentsburg than in Ny-Ålesund. A few rare, but powerful outflows of smoke aerosol have led to an increase in the Monthly $\tau_{0.5}^{f}$ (Fig. 10) and $\tau_{0.5}^{a}$ (Fig. 8) values and distorted the natural seasonal variations. After the events of smoke outflows are eliminated (see dashed lines in Figs. 8 and 10), the seasonal AOD behavior in Barentsburg becomes similar to that in Ny-Ålesund, but with larger (by 0.017, on the average) AOD values. The average AOD characteristics for the periods of spring maximum and fall minimum in the two regions are presented in Table 4 and in Fig. 11.

Table 4. Average AOD characteristics (± SD) in Ny-Ålesund and Barentsburg during spring (April-May) maximum (first row) and fall (August-September) minimum (second row)

Characteristics	Ny-Ålesund, 2002-2018	Ny-Ålesund, 2011-2018	Barentsburg, 2011-2018 (No smoke)
$\tau_{0.5}^{a}$	0.081±0.03 0.052±0.023	0.070±0.015 0.052±0.015	0.086±0.012 0.070±0.022
$\tau_{0.5}^{f}$	0.062±0.024 0.038±0.019	0.054±0.012 0.038±0.013	0.063±0.012 0.048±0.02
τ^{c}	0.019±0.007 0.014±0.004	0.016±0.005 0.014±0.003	0.022±0.009 0.022±0.011
α	1.43±0.23 1.38±0.26	1.47±0.22 1.35±0.30	1.33±0.28 1.17±0.36
β	0.031±0.01 0.02±0.008	0.026±0.007 0.02±0.005	0.035±0.008 0.032±0.012

375 From Fig. 10 and Table 4 it can be seen that the fine component makes the major contribution to the formation of the seasonal AOD behavior: the average $\tau_{0.5}^{f}$ values decrease from spring toward fall in the two regions by almost the same amount of 0.015-0.016. Also, modal (most probable) $\tau_{0.5}^{f}$ values vary in a similar way (Fig. 12a). The $\tau_{0.5}^{f}$ mode from spring toward fall shifts from 0.07 to 0.03 in Barentsburg and from 0.05 to 0.03 in Ny-Ålesund. Average (Fig. 10) and modal (Fig. 12b) values of coarse AOD component remain almost unchanged during the polar day: Monthly τ^{c} values are about 0.015 in Ny-

380 Ålesund and 0.022 in Barentsburg.

Seasonal decrease of $\tau_{0.5}^{f}$ from spring toward fall leads to changes in the ratio ($\tau_{0.5}^{f} / \tau^{c}$) and spectral AOD dependence (Fig. 11): the slope of the spectral AOD dependence and the Ångström exponent become a little smaller. The relative contribution of fine aerosol to AOD ($\tau_{0.5}^{f} / \tau_{0.5}^{a}$) in Ny-Ålesund is 0.77 in spring and 0.73 in fall. In Barentsburg this ratio is a little smaller, 0.73 and 0.69 respectively.

385

4 Conclusions

We present brief results of our study.

1. It is noted that, to identify the specific features of seasonal and multiyear variations in atmospheric AOD, it is important

390 to analyze separately fine and coarse AOD components, having different spectral properties, origins, and lifetimes. As applied

to AOD measurements in Ny-Ålesund, we considered a few methods for estimating the contributions of fine and coarse components, and one of the methods (IM1) is selected for a subsequent use. A comparison with data from the base (EM) showed that the standard deviation of the τ^c and $\tau_{0.5}^f$ calculations is 0.007, and the relative errors are 30% and 11% respectively.

395   2. Outflows of fine aerosol of different types from the Eurasian and North American midlatitudes affect appreciably the monthly (and even annual) AOD in the Arctic atmosphere. Outflows of smokes from massive forest and agricultural fires have the strongest effect. The frequency of these episodic outflows in specific years, as well as the frequency of situations of Arctic haze, influence the specific features of seasonal variations and determine the amplitude of interannual AOD variations in the Arctic atmosphere.

400   3. The oscillations in annual AOD in Ny-Ålesund and Barentsburg are coordinated in character and determined by fine aerosol (interannual variations in τ^c are a factor of 2-3 smaller). In the multiyear (2002-2018) variations we revealed a tendency of decreasing AOD, but the trend is statistically insignificant. Annual AOD in Barentsburg is, on the average, 0.02 larger than in Ny-Ålesund, indicating larger contents of both fine ($\Delta\tau_{0.5}^f = 0.012$) and coarse ($\Delta\tau^c = 0.008$) aerosol in the bigger settlement.

4. The seasonal AOD variations in Ny-Ålesund are characterized by a decrease from spring toward fall. In the last period 405   (2011-2018) the seasonal AOD decrease became less pronounced. Monthly AOD values decreased from 0.07-0.09 by the amount of ~0.02 in March-June, and remained unchanged (0.05-0.06) in the second half of polar day. In the seasonal AOD variations in Barentsburg there had been an additional summer maximum, caused by a relatively larger influence of smoke outflows. After smoke outflow events are eliminated, the seasonal behaviour becomes analogous to that in Ny-Ålesund, but with (0.017) higher AOD values.

410   5. Fine component has the main effect on the formation of seasonal behaviour of AOD. Its relative contribution to AOD ($\tau_{0.5}^f$ / $\tau_{0.5}^a$) is 0.77 in spring and 0.73 in fall in Ny-Ålesund (0.73 and 0.69 in Barentsburg). Coarse AOD component during the polar day is almost unchanged, being, on the average, 0.015 in Ny-Ålesund and 0.022 in Barentsburg. The average annual and monthly values of the Ångström exponent α (from 1.2 to 1.5) do not differ from those at the midlatitudes of the continental atmosphere. That large exponents α are because the ratios of the two AOD components ($\tau_{0.5}^f$ / τ^c) differ little between the Arctic 415   and continental atmosphere.

Acknowledgements

The authors thank all our colleagues who organized and carried out the photometric observations in Ny-Ålesund and Barentsburg, namely, to S. Debatin, J. Graeser, D.G. Chernov, A.V. Gubin, K.E. Lubo-Lesnichenko, A.N. Prakhov, V.F. 420   Radionov, O.R. Sidorova, and Yu.S. Turchinovich.

The study was supported by the Ministry of Science and Higher Education of the Russian Federation (Project No AAAA-A17-117021310142-5)

References

425   Alexandov, M. D., Marshak, A., Cairns, B., Lacis, A. A., Carlson, B.E. Automated cloud screening algorithm for MFRSR data, Geophys. Res. Lett., Vol. 31, L04118, doi: 10.1029/2003GL019105, 2004

Anderson, G., Clough, S., Kneizys, F., Chetwynd, J., and Shettle, E. AFGL Atmospheric Constituent Profiles (0 – 120 km), Air Force Geophysics Laboratory // AFGL-TR-86-0110. Environmental Research Paper No. 954., 1986

Angstrom A. Parameters of atmospheric turbidity // Tellus XVI. 1964, N 1, p. 64-75.

430   Cachorro V.E., Duran P., Vergaz R. and de Frutos A.M. Measurements of the atmospheric turbidity of the north-centre continental area in Spain: spectral aerosol optical depth and Angstrom turbidity parameters // J. Aerosol Sci. 2000, Vol. 31, No. 6, pp. 687-702.

Chen Y.-C., Hamre B., Frette Q., Muyimbwa D., Blindheim S., Stebel K., Sobolewski P., Toledano C., Stamnes J. Aerosol optical properties in Northern Norway and Svalbard, Applied Optics, Vol. 55, No 4. p. 660-672. doi: 435   10.1364/AO.55.000660, 2016

Chubarova N., Nezval' Ye., Sviridenkov M., Smirnov A., Slutsker I. Smoke aerosol and its radiative effects during extreme fire event over Central Russia in summer 2010, Atmospheric Measurement Techniques, V. 5, p. 557-568. doi:10.5194/amt-5-557-2012, 2012

Chubarova N.E., Nezval' E.I., Belikov I.B., Gorbarenko E.V., Eremina I.D., Zhdanova E.Yu., Korneva I.A., Konstantinov 440   P.I., Lokoshchenko M.A., Skorokhod A.I., Shilovtseva O.A. Climatic and Environmental Characteristics of Moscow Megalopolis According to the Data of the Moscow State University Meteorological Observatory over 60 Years, Russian Meteorology and Hydrology, Vol. 39, No. 9, pp. 602–613. doi: 10.3103/S1068373914090052, 2014

Chubarova N.Y., Poliukhov A.A., Gorlova I.D. Long-term variability of aerosol optical thickness in Eastern Europe over 2001–2014 according to the measurements at the Moscow MSU MO AERONET site with additional cloud and NO 2 445   correction, Atmospheric Measurement Techniques, Vol. 9. No 2. p. 313-334. https://doi.org/10.5194/amt-9-313-2016, 2016

Eck, T.F., Holben B.N., Reid J.S., Dubovik O., Smirnov A., O'Neill N.T., Slutsker I., and Kinne S. Wavelength dependence of the optical biomass burning, urban, and desert dust aerosol // J. Geophys. Res., 1999, Vol. 104, 31333-31350.

Eck, T.F., Holben B.N., Reid J.S., Sinyuk A., Hyer E.J., O'Neill N.T., Shaw G.E., Vande Castle J.R., Chapin F.S., Dubovik 450   O., Smirnov A., Vermote E., Schafer J.S., Giles D., Slutsker I., Sorokine M., and Newcomb W.W. Optical properties of boreal region biomass burning aerosols in central Alaska and seasonal variation of aerosol optical depth at an Arctic coastal site, J. Geophys. Res., Vol. 114, D11201. doi:10.1029/2008JD010870, 2009

Freund J. Aerosol optical depth in the Canadian Arctic, Atmos. – Ocean, Vol. 21, No 2, p. 158-167, 1983

Glantz, P., Bourassa A., Herber A., Iversen T., Karlsson J., Kirkevåg A., Maturilli M., Seland Ø., Stebel K., Struthers H.,
455   Matthias M., and Thomason L. Remote sensing of aerosols in the Arctic for an evaluation of global climate model
simulations, J. Geophys. Res. Atmos., 119, p. 8169–8188, doi:10.1002/2013JD021279, 2014

Gorbarenko E.V., Rublev A.N. Long-term changes in the aerosol optical thickness in Moscow and correction under strong
atmospheric turbidity, Izvestiya, Atmospheric and Oceanic Physics. 2016. Vol. 52. No. 2. p. 188-195.

Herber A., Thomason L.W., Gernandt H., Leiterer U., Nagel D., Schulz K., Kaptu J., Albrecht T., Notholt J. Continuous day
460   and night aerosol optical depth observations in the Arctic between 1991 and 1999, Journal of Geophysical Research. 107,
D10, 4097, doi:10.1029/2001JD000536, 2002

Hoffmann A., Ritter C., Stock M., Maturilli M., Eckhardt S., Herber A., and Neuber R. Lidar measurements of the Kasatochi
aerosol plume in August and September 2008 in Ny-Ålesund, Spitsbergen, Journal of Geophysical Research, 2010, 115,
D00L12, doi:10.1029/2009JD013039, 2010

465 Holben B.N., Eck T.F., Slutsker I., Tanre D., Buis J.P., Setzer A., Vermote E., Reagan J.A., Kaufman Y.J., Nakadjima T.,
Lavenu F., Jankowiak I., and Smirnov A. AERONET - A federated instrument network and data archive for aerosol
characterization, Rem. Sens. Env., 1998, 66(1), P. 1-16., 1988

Holben B.N., Tanre D., Smirnov A., Eck T.F., Slutsker I., Abuhassan N., Newcomb W.W., Schafer J.S., Chatenet B., Lavenu
F., Kaufman Y.J., J. Vande Castle, Setzer A., Markham B., Clark D., Frouin R. Halthore R., Karneli A., O'Neill N.T.,
470   Pietras C., Pinker R.T., Voss K., and Zibordi G. An emerging ground-based aerosol climatology: Aerosol optical depth
from AERONET // Journal of Geophysical Research. Vol. 106. No. D11, p. 12,067-12,097. doi: 10.1016/S0034-
4257(98)00031-5, 2001

IPCC: Climate Change 2013: The Physical Science Basis, Intergovernmental Panel on Climate Change, 2013. 1552 p.
[Electronic resource]. URL: http://www.climatechange2013.org/images/report/WG1AR5_ALL_FINAL.pdf. 2013

475 Isaksen, K.; Nordli, O.; Forland, E.J.; Lupikasza, E.; Eastwood, S. and Niedzwiedz, T. Recent warming on Spitsbergen—
Influence of atmospheric circulation and sea ice cover, J. Geophys. Res. Atmos., 121, 11,913–11,931, doi:
10.1002/2016JD025606. 2016

Kabanov D.M., Sakerin S.M. About method of atmospheric aerosol optical thickness determination in near-spectral range,
Atmospheric and Oceanic Optics. Vol. 10, No 8, p. 540-545, 1997

480 Kabanov D.M., Veretennikov V.V., Voronina Yu.V., Sakerin S.M., Turchinovich Yu.S. Information system for network
sunphotometers // Atmospheric and oceanic optics, Vol. 22, No. 1, p. 121-127, doi:10.1134/S1024856009010187, 2009.

Kabanov D.M., Sakerin S.M. Comparison of assessment techniques of fine and coarse component aerosol optical depth of the
atmosphere from measurement in the visible spectrum, 22nd International Symposium Atmospheric and Ocean Optics:
Atmospheric Physics. Proceedings of SPIE. Vol. 10035. Part 1. 1003 3D [10035-46], 2016.

485 Kabanov D.M., Sakerin S.M., Kruglinsky I.A., Ritter C., Sobolewski P.S., Zielinski T. Comparison of atmospheric aerosol
optical depths measured with different sun photometers in three regions of Spitsbergen Archipelago, Proc. SPIE 10833,

24th International Symposium on Atmospheric and Ocean Optics: Atmospheric Physics, 1083342 (13 December 2018); doi: 10.1117/12.2503949, 2018

Kabanov D.M., Sakerin S.M., Ritter C. Preparing time series of observations of atmospheric aerosol optical depth (AOD) at two stations on Spitsbergen Archipelago and selecting methods of extracting the contributions of fine and coarse AOD components, Proc. SPIE. 11208, 25th International Symposium on Atmospheric and Ocean Optics: Atmospheric Physics, 112083E (18 December 2019), doi: 10.1117/12.2539926, 2019.

Kabanov D.M., Sakerin S.M., Turchinovich Yu.S. Interannual and seasonal variations in the atmospheric aerosol optical depth in the region of Tomsk over 24 years of observations, Atmospheric and oceanic optics, 2019b, Vol. 32, No 7, р. 548-555. doi: 10.15372/AOO201907 [in Russian].

Kasten F., Young A.T. Revised optical air mass tables and approximation formula, Appl. Opt. 28 (22), 4375-4738, doi: 10.1364/AO.28.004735, 1989

Kondratyev K.Ya., Ivlev L.S., Krapivin V.F., Varotsos C.A. Atmospheric aerosol properties, formation processes, and impacts: from nano- to global scales, Springer/PRAXIS, Chichester, U.K. 572 pp., 2006

Li J., Carlson B.E., Dubovik O., Lacis A.A. Recent trends in aerosol optical properties derived from AERONET measurements, Atmospheric Chemistry and Physics Vol. 14. No. 22. p. 12271-12289. www.atmos-chem-phys.net/14/12271/2014/doi:10.5194/acp-14-12271-2014, 2014

Markowicz K.M., Pakszys P., Ritter C., Zielinski T., Udisti R., Cappelletti D., Mazzola M., Shiobara M., Xian P., Zawadzka O., Lisok J., Petelski T., Makuch P., Karasiński G. Impact of North American intense fires on aerosol optical properties measured over the European Arctic in July 2015, J. Geophys. Res. Atmos. Vol 121, p. 14487-14512, http://dx.doi.org/10.1002/2016JD025310, 2016.

Mazzola, M.; Stone, R.S.; Herber, A.; Tomasi, C.; Lupi, A.; Vitale, V.; Lanconelli, C., Toledano, C.; Cachorro, V.E.; O'Neill, N.T.; Shiobare, M.; Aaltonen, V. et al. Evaluation of sun photometer capabilities for retrievals of aerosol optical depth at high latitudes: The POLAR-AOD intercomparison campaigns. Atmosph. Environm. doi: 10.1016/j.atmosenv.2011.07.042. 2011

Michalsky J., Denn F., Flynn C., Hodges G,, Kiedron P., Koontz A., Schlemmer J., and Schwartz S.E. Climatology of aerosol optical depth in north-central Oklahoma: 1992–2008, J. Geophys. Res., 2010, Vol. 115, D07203, doi:10.1029/2009JD012197, 2010.

Myhre C.L., Toledano C., Myhre G., Lihavainen H. Regional aerosol optical properties and radiative impact of the extreme smoke event in the European Arctic in spring 2006, Atmos. Chem. Phys., 2007, 7 (22), p. 511-534, http://dx.doi.org/10.5194/acp-7-5899-2007.

Ohvril H., Teral H., Neiman L., Uustare M., Tee M., Russak V., Kallis A., Okulov O., Terez E., Terez G., Guschin G., Abakumova G., Gorbarenko E., Tsvetkov A., and Laulainen N. Global dimming and brightening versus atmospheric column transparency, Europe, 1906–2007, J. Geophys. Res. 114, D00D12, doi:10.1029/2008JD010644, 2009.

520 O'Neill N.T., Eck T.F., Smirnov A., Holben B.N., and Thulasiraman S. Spectral discrimination of coarse and fine mode optical depth, J. Geophys. Res. 108(D17), 4559-4573, doi:10.1029/2002JD002975, 2003.

Pakszys P., Zielinski T. Aerosol optical properties over Svalbard: a comparison between Ny-Ålesund and Hornsund, Oceanologia, 2017, 59, p. 431-444. http://dx.doi.org/10.1016/j.oceano.2017.05.002, 2017.

Plakhina I.N., Pankratova N.V., and Makhotkina E.L. Variations in the atmospheric aerosol optical depth from the data
525 obtained at the Russian actinometric network in 1976–2006, Izv. Atmos. Ocean. Phys. 45 (4), p. 456–466, 2009.

Putaud J.P., Cavalli F., Martins dos Santos S., and Dell'Acqua A. Long-term trends in aerosol optical characteristics in the Po Valley, Italy, Atmos. Chem. Phys. 14, p. 9129–9136, doi:10.5194/acp- 14-9129-2014, 2014.

Radionov V.F., and Marshunova M.S. Long-term variations in the turbidity of the Arctic atmosphere in Russia, Atmos. Ocean, 30(4), p. 531-549, 1992.

530 Quinn, P., Shaw, G., Andrews, E., Dutton, E.G., Ruoho-Airola, T., Gong, S.L. Arctic haze: current trends and knowledge gaps // Tellus, 59B (1), p. 99–114. http://dx.doi.org/10.1111/j.1600-0889.2006.00238.x, 2007.

Sakerin S.M. and Kabanov D.M. Spectral dependence of the atmospheric aerosol optical depth in the wavelength range from 0.37 to 4 μm, Atmos. Ocean. Opt., Vol. 20, No 2, p. 141–149, 2007a

Sakerin S.M., Kabanov D.M. Correlations between the parameters of Angström formula and aerosol optical thickness of the
535 atmosphere in the wavelength range from 1 to 4 μm, Atmospheric and oceanic optics, Vol. 20, No 3, p. 200-206, 2007b.

Sakerin S.M., Gorbarenko E.V., and Kabanov D.M. Peculiarities of many-year variations of atmospheric aerosol optical thickness and estimates of influence of different factors, Atmospheric and Oceanic Optics. Vol. 21, No 7, p. 540–545, 2008a.

Sakerin S.M., Kabanov D.M., Smirnov A.V., Holben B.N. Aerosol optical depth of the atmosphere over ocean in the
540 wavelength range 0.37-4 μm, International J. Remote Sensing, Vol. 29, Issue 9. p. 2519-2547. doi: 10.1080/01431160701767492, 2008b.

Sakerin S.M., Kabanov D.M., Nasrtdinov I.M., Turchinovich S.A., and Turchinovich Yu.S. The results of two-point experiments on the estimation of the urban anthropogenic effect on the characteristics of atmospheric transparency // Atmospheric and Oceanic Optics, Vol. 23, No. 2, p. 88–94. doi: 10.1134/S1024856010020028. 2010

545 Sakerin S.M., Kabanov D.M., Rostov A.P., Turchinovich S.A., and Knyazev V.V. Sun photometers for measuring spectral air transparency in stationary and mobile conditions, Atmos. Ocean. Opt. Vol. 26, No 4, p. 352–356. doi: 10.1134/S102485601304012X, 2013.

Sakerin S.M., Beresnev S.A., Kabanov D.M., Kornienko G.I., Nikolashkin S.V., Poddubny V.A., Tashchilin M.A., Turchinovich Yu.S., Holben B.N., and Smirnov A. Analysis of approaches to modeling the annual and spectral behaviors
550 of atmospheric aerosol optical depth in Siberia and Primorye, Atmospheric and Oceanic Optics, Vol. 28, No. 2, p. 145–157. DOI: 10.1134/S1024856015020104, 2015.

Sakerin S.M., Kabanov D.M., Radionov V.F., Chernov D.G., Turchinovich Yu.S., Lubo-Lesnichenk K.E., and Prakhov A.N. Generalization of results of atmospheric aerosol optical depth measurements on Spitsbergen Archipelago in 2011–2016,

Atmospheric and Oceanic Optics, Vol. 31, No. 2, p. 163–170. doi: 10.1134/S1024856018020112, 2018a.

555 Sakerin S.M., Golobokova L.P., Kabanov D.M., Pol'kin V.V., and Radionov V.F. Zonal distribution of aerosol physicochemical characteristics in the Eastern Atlantic, Atmospheric and Oceanic Optics, Vol. 31, No. 5, pp. 492–501. DOI: 10.1134/S1024856018050160, 2018b.

Schuster, G.L., Dubovik O., and Holben B.N. Angstrom exponent and bimodal aerosol size distributions // J. Geophys. Res., 2006, Vol. 111, D07207. doi:10.1029/2005JD006328.

560 Shaw G.E. Atmospheric turbidity in the Polar regions, Journal of Applied Meteorology, Vol. 21, p. 1080-1088 doi: 10.1175/1520-0450(1982)021<1080:ATITPR>2.0.CO;2, 1982.

Shaw G.E. The Arctic haze phenomenon, Bull. Amer. Meteor. Soc., Vol. 76, No 12, p. 2403–2414 doi: 10.1175/1520-0477(1995)076<2403:TAHP>2.0.CO;2, 1995.

Shifrin K.S. Simple relationships for the Angstrom parameter of disperse systems // Appl. Opt., 1995, Vol. 34, 4480-4485.

565 Sitnov S.A., Gorchakov G.I., Sviridenkov M.A., Gorchakova I.A., Karpov A.V., and Kolesnikova A.B. Aerospace monitoring of smoke aerosol over the European part of Russia in the period of massive forest and peatbog fires in July–August of 2010, Atmospheric and Oceanic Optics, Vol. 26, No. 4, p. 265-280. doi: 10.1134/S1024856013040143, 2013.

Stohl A., Andrews E., Burkhart J.F., Forster C., Herber A., Hoch S.W., Kowal D., Lunder C., Mefford T., Ogren J.A., Sharma S., Spichtinger N., Stebel K., Stone R., Stro¨m J., Tørseth K., Wehrli C., and Yttri K.E. Pan-Arctic enhancements of light absorbing aerosol concentrations due to North American boreal forest fires during summer 2004, J. Geophys. Res., 2006a, Vol. 111, D22214, doi: 10.1029/2006JD007216, 2006a.

Stohl A., Berg T., Burkhart J.F., Fjǽraa A.M., Forster C., Herber A., Hov Ø., Lunder C., McMillan W.W., Oltmans S., Shiobara M., Simpson D., Solberg S., Stebel K., Ström J., Tørseth K., Treffeisen R., Virkkunen K., Yttri K.E. Arctic smoke – record high air pollution levels in the European Arctic due to agricultural fires in Eastern Europe in spring 2006, Atmos. Chem. Phys. Vol. 7, No 2, p. 511-534, http://dx.doi.org/10.5194/acp-7-511-2007, 2007.

Stone R.S., Anderson G.P., Shettle E.P., Andrews E., Loukachine K., Dutton E.G., Schaaf C., Roman III M.O. Radiative impact of boreal smoke in the Arctic: Observed and modelled, J. Geophys. Res., 113, D14S16. http://dx.doi.org/10.1029/2007JD009657, 2008.

Sviridenkov M.A. Retrieval of atmospheric aerosol characteristics from spectral measurements of transparency and small-angle scattering // Atmos. Ocean. Opt. Vol. 14, No 12, p. 1022–1025, 2001.

Toledano C., Cachorro V., Gausa M., Stebel K., Aaltonen V., Berjon A., Ortis J.P., de Frutos A.M., Bennouna Y., Blindheim S., Myhre C.L., Zibordi G., Wehrli C., Kratzer S., Hakanson B., Carlund T., de Leuww G., Herber A. Overview of sun photometer measurements of aerosol properties in Scandinavia and Svalbard // Atmospheric Environment, Vol. 52, p. 18-28. doi:10.1016/j.atmosenv. 2011.10.022, 2012.

585 Tomasi C., Lupi A., Mazzola M., Stone R.S., Dutton E.G., Herber A., Radionov V.F., Holben B., Sorokin M., Sakerin S.M., Terpugova S.A., Lanconelli C., Petkov B., and Vitale V. An update of the long-term trend of aerosol optical depth in the polar regions using POLAR-AOD measurements performed during in International Polar Year, Atmospheric

Environment, 52, p. 29-47. doi:10.1016/j.atmosenv2012.02.055, 2012.

590 Tomasi C., Kokhanovsky A.A., Lupi A., Ritter C., Smirnov A., Mazzola M., Stone R.S., Lanconelli C., Vitale V., Holben B.N., Nyeki S., Wehrli C., Altonen V., de Leeuw G., Rodriguez E., Herber A.B., Stebel K., Stohl A., O'Neill N.T., Radionov V.F., Zielinski T., Petelski T., Sakerin S.M., Kabanov D.M., Xue Y., Mei L., Istomina L., Wagener R., McArthur B., Sobolewski P.S., Butler J., Kivi R., Courcoux Y., Larouche P., Broccardo S., Piketh S.J. Aerosol remote sensing in polar regions, Earth-Science Reviews. Vol. 140. p. 108–157. http://dx.doi.org/10.1016/j.earscirev.2014.11.001, 2015.

595 Tørseth K., Aas W., Breivik K., Fjæraa A.M., Fiebig M., Hjellbrekke A.G., Lund Myhre C., Solberg S., and Yttri K.E. Introduction to the European Monitoring and Evaluation Programme (EMEP) and observed atmospheric composition change during 1972–2009, Atmospheric Chemistry and Physics. Vol. 12. №. 12. p. 5447-5481. www.atmos-chem-phys.net/12/5447/2012/ doi:10.5194/acp-12-5447-2012, 2012.

Twitty J.T. The inversion of aureole measurements to derive aerosol size distributions, J. Atm. Sci. V. 32. p. 584-591, doi:
600 10.1175/1520-0469(1975)032<0584:TIOAMT>2.0.CO;2, 1975.

Vinogradova A.A., Smirnov N.S., Korotkov V.N., and Romanovskay A.A. Forest fires in Siberia and the far east: emissions and atmospheric transport of black carbon to the Arctic, Atmospheric and Oceanic Optics, Vol. 28, No. 6, p. 566–574. doi: 10.1134/S1024856015060184, 2015.

Walczowski, W.; Piechura, J. Influence of the West Spitsbergen Current on the local climate. Int. J. Climatol. 31: 1088–1093,
605 doi: 10.1002/joc.2338. (2011)

Weller M., Schulz E., Leiterer U., Naebert T., Herber A., and Thomason L.W. Ten years of aerosol optical depth observation at the Lindenberg meteorological observatory, Contr. Atmos. Phys. Vol. 71, No. 4, p. 387-400, 1998.

WMO/GAW Expert Workshop on a global surface-based network for long term observations of column aerosol optical properties, Eds. U Baltensperger, L. Barrie, C. Wehrli. Report GAW 162 - WMO/GAW. Davos, March' 05. (WMO TD
610 No. 1287), 2005, 144 p. http://library.wmo.int/pmb_ged/wmo-td_1287.pdf.

WMO / GAW report no. 183, operations handbook - ozone observations with a Dobson spectrophotometer, 2008, URL https://www.wmo.int/pages/prog/arep/gaw/documents/GAW183-Dobson-WEB.pdf

Xia, X.G. Variability of aerosol optical depth and Ångström wavelength exponent derived from AERONET observations in recent decades, Environ. Res. Lett. 6, 044011, doi:10.1088/1748- 9326/6/4/044011, 2011.

615 Zhdanova E.Yu., Khlestova Yu.O., Chubarova N.Y. Trends in characteristics of atmospheric aerosols in Moscow based on long-term AERONET observations, Atmospheric and Oceanic Optics Vol. 32, No 6, p: 443-448, doi: 10.15372/AOO20190604 [in Russian], 2019.

Zhuravleva T., Kabanov D., Nasrtdinov I., Russkova T., Sakerin S., Smirnov A., and Holben B. Radiative characteristics of aerosol under smoke mist conditions in Siberia during summer 2012, Atmos. Meas. Tech. Vol. 10, p. 179-198.
620 http://www.atmos-meas-tech.net/10/179/2017. doi:10.5194/amt-10-179-2017, 2017.

The *Figures*
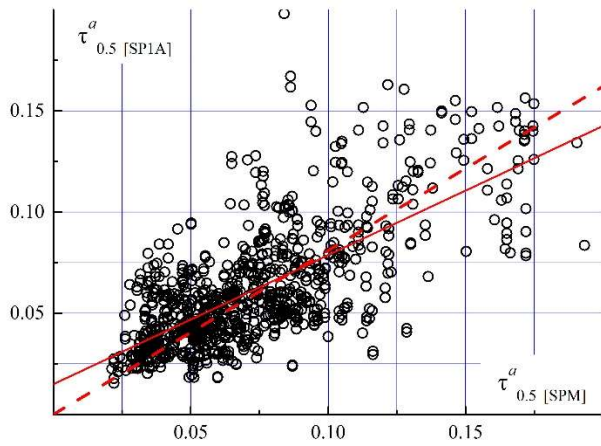
Fig. 1. Scatter diagram of AOD measurements in two regions using SP1A (Ny-Ålesund) and SPM (Barentsburg) photometers. Solid line: unconstrained linear regression; dotted line: regression through origin (0,0)

625
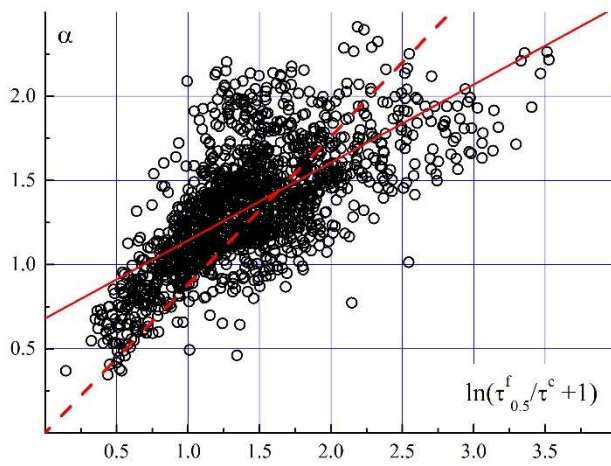
Fig. 2. Correlation dependence between the exponent α and the ratio $\left(\tau_{0.5}^{f} / \tau^{c} \right)$ according to measurements in Barentsburg. Solid line: unconstrained linear regression; dotted line: regression through origin (0,0)

630
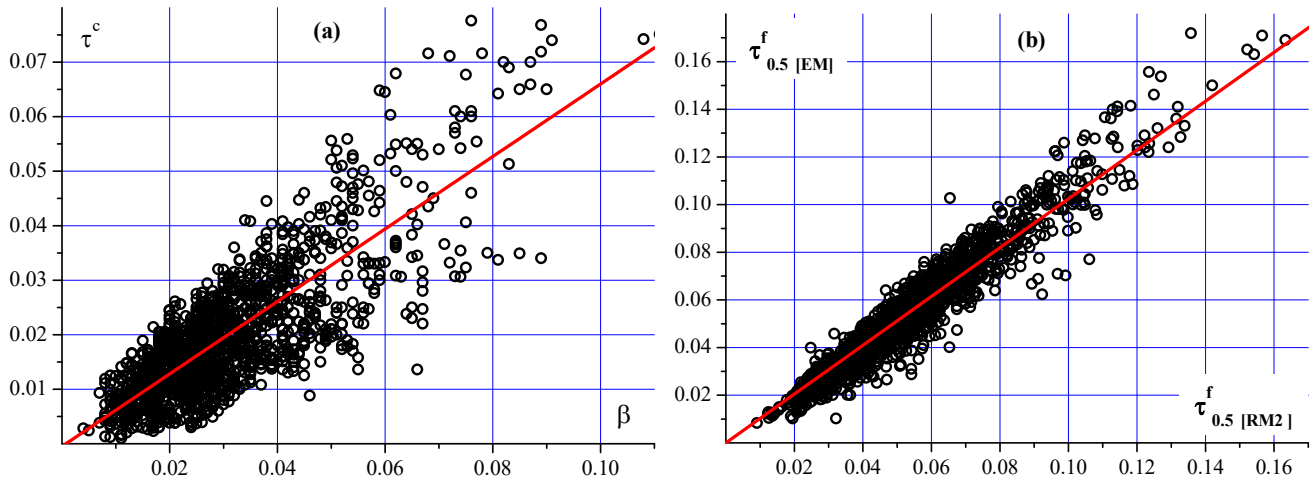
Fig. 3. (a) Interrelation of τ^c with the parameter β and (b) interrelation of $\tau^f_{0.5}$, calculated using the base (EM) and RM2 methods
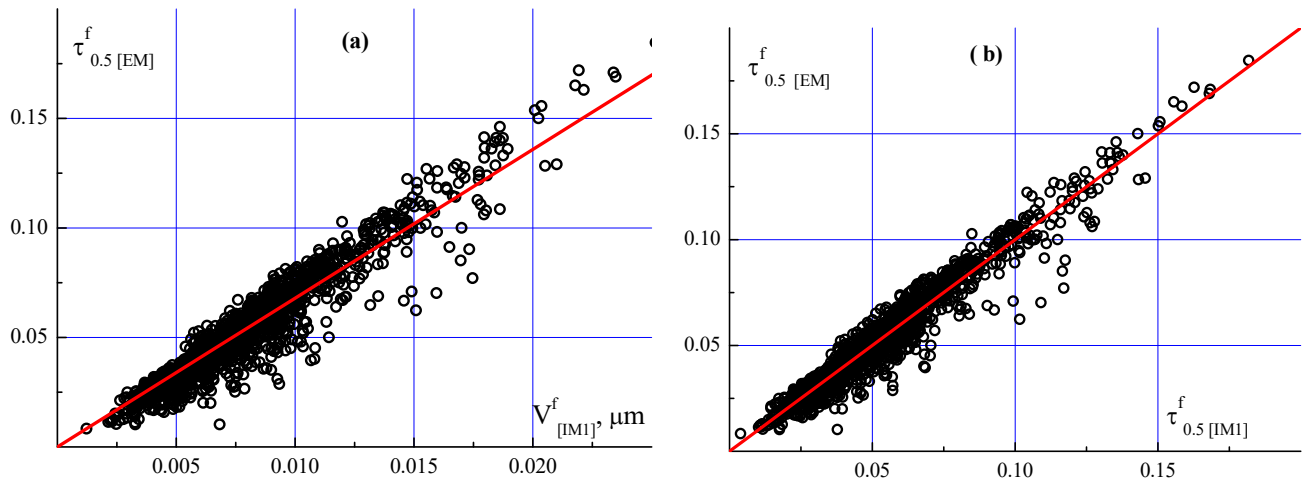
Fig. 4. (a) Interrelation between $\tau^f_{0.5}$ and particle volume V^f and (b) interrelation between $\tau^f_{0.5}$ values, calculated using inversion (IM1) and
635   empirical (EM) methods
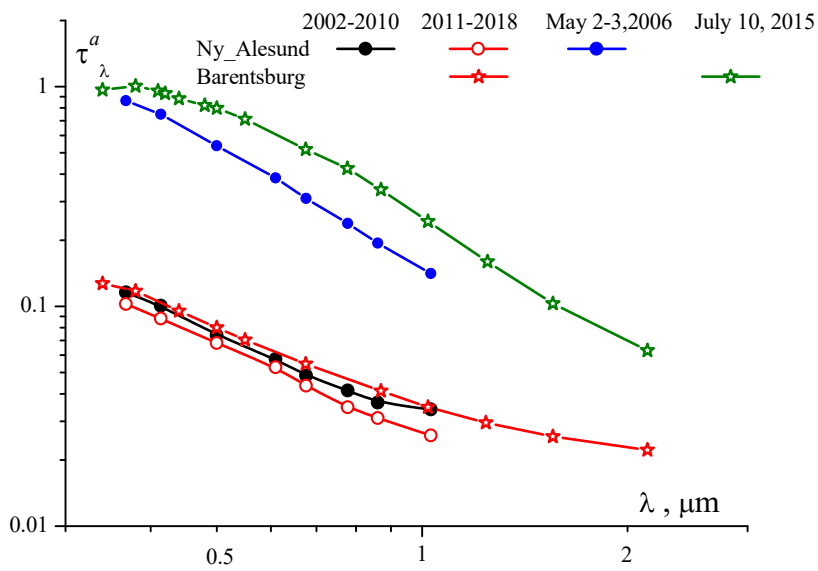
Fig. 5. Spectral dependences of AOD: at the top shows situations with high aerosol turbidities of the atmosphere; and the bottom shows multiyear averages in two regions
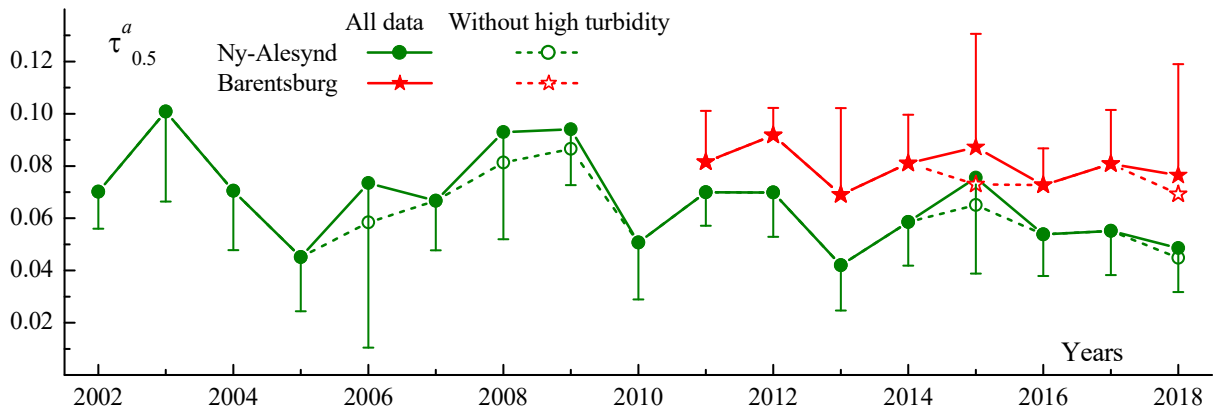
640   Fig. 6. Multiyear variations in Annual AOD in Ny-Ålesund and Barentsburg
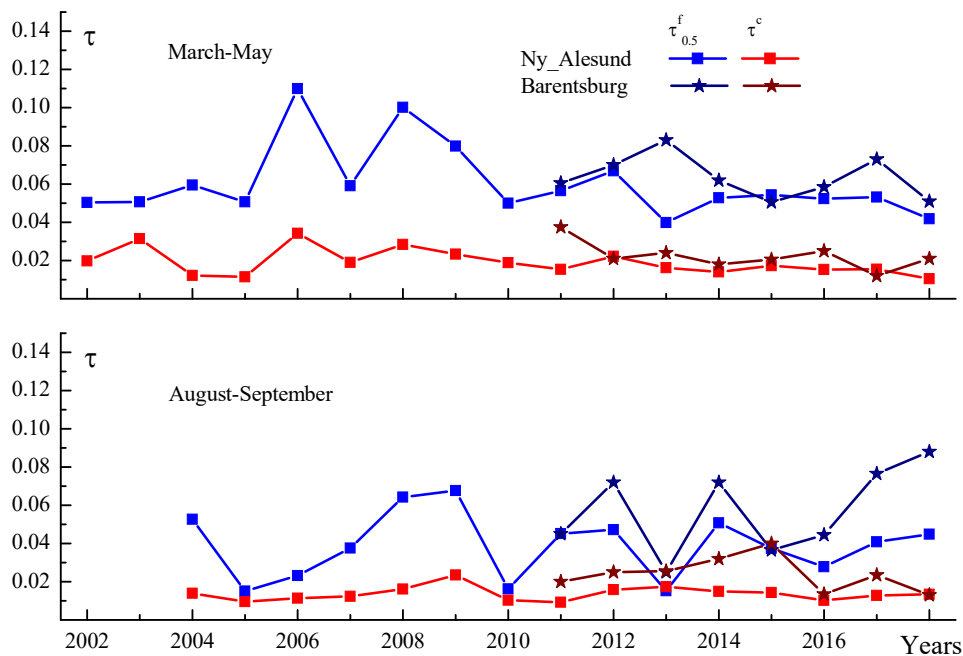
Fig. 7. Multiyear variations in $\tau_{0.5}^{f}$ and τ^{c} for the periods of spring maximum and fall minimum of AOD in two regions of Spitsbergen
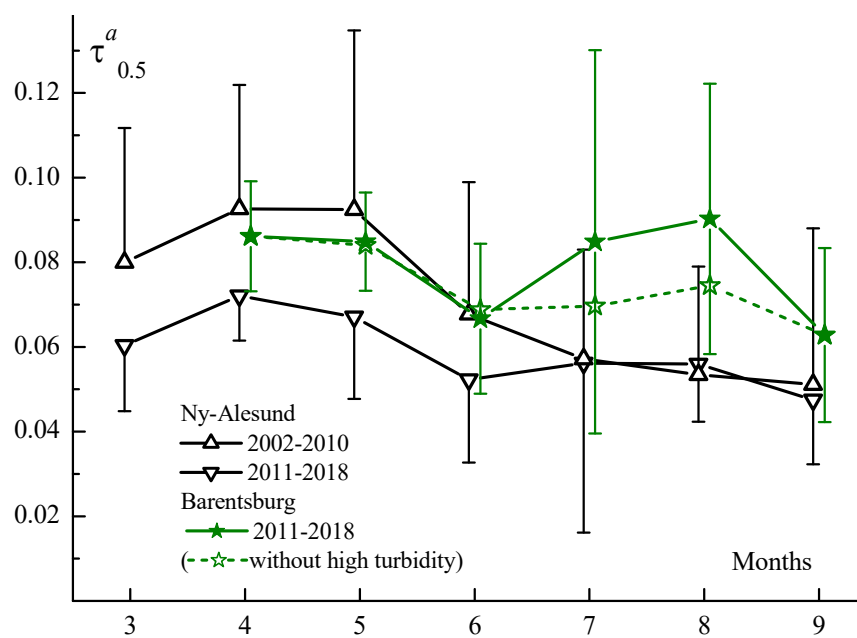
Fig. 8. Seasonally average $\tau_{0.5}^{a}$ variations in Ny-Ålesund and Barentsburg
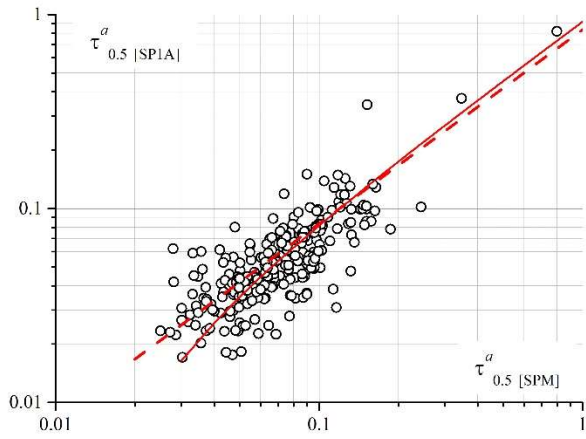
645

Fig. 9. Interrelation between daily AOD (0.5 μm) values, measured in Ny-Ålesund and Barentsburg (2011-2018). Solid line: unconstrained linear regression; dotted line: regression through origin (0,0)
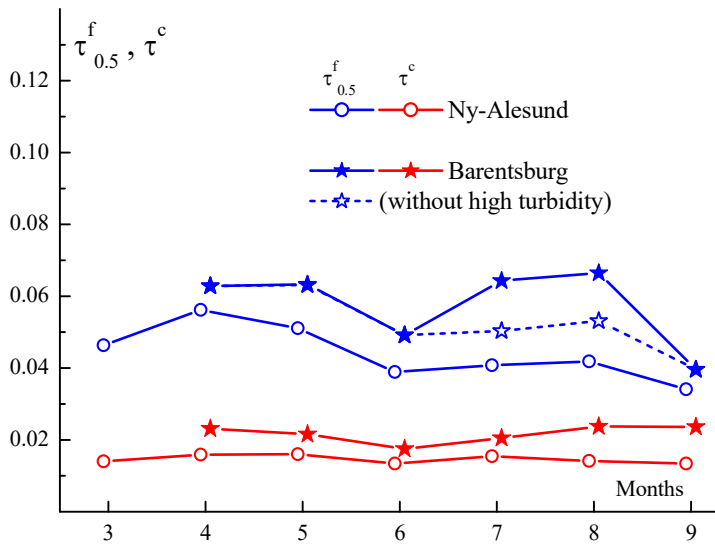
650   Fig. 10. Seasonal variations in fine and coarse AOD components in Ny-Ålesund and Barentsburg
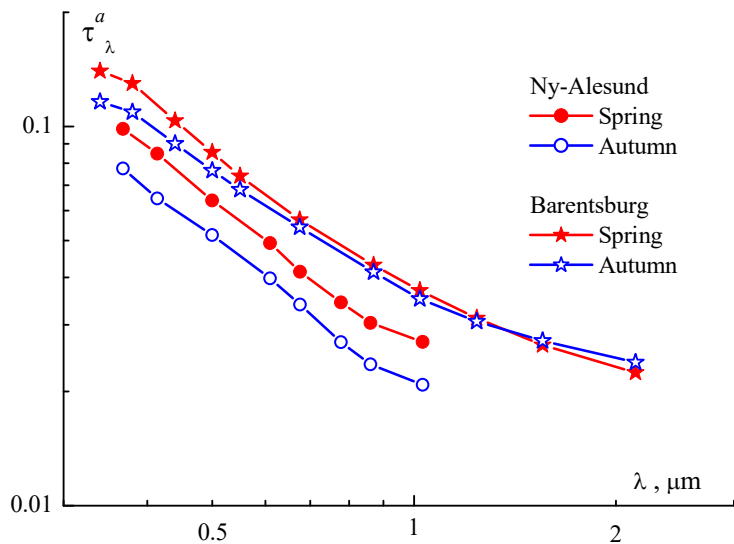
Fig. 11. Average spectral dependences of AOD in two regions of Spitsbergen (2011-2018) during spring (April-May) maximum and fall (August-September) minimum

655
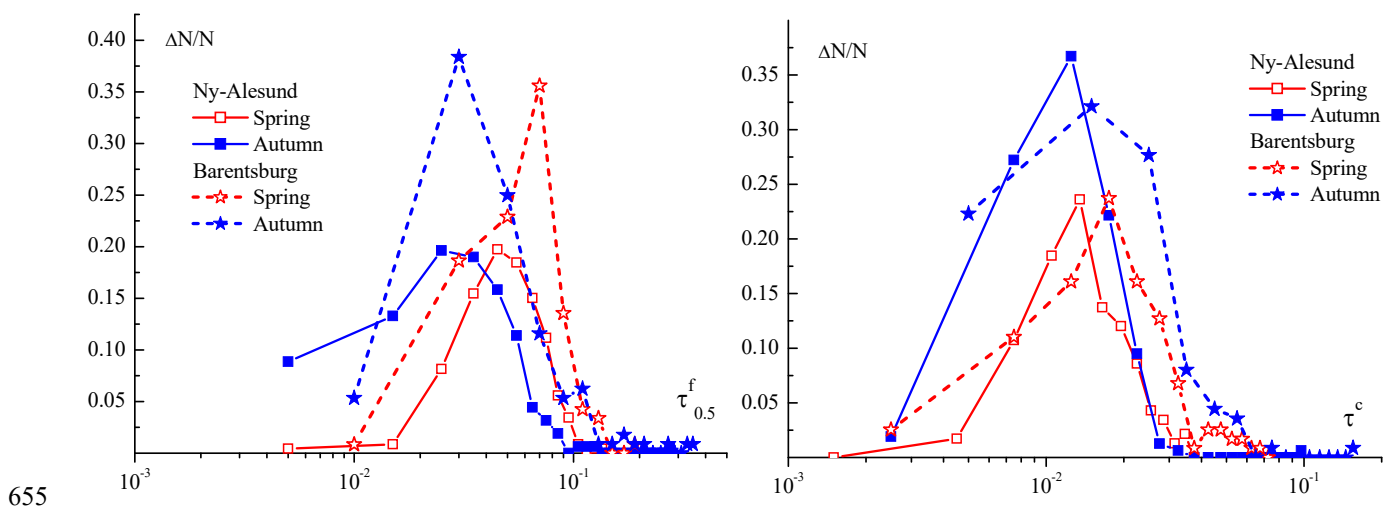
Fig. 12. Frequency histograms of (a) $\tau_{0.5}^{f}$ and (b) τ^{c} in spring and fall in two regions of Spitsbergen (2011-2018)

660

665

logo of Copernicus Publications.